Terahertz plasmon and surface-plasmon modes in cylindrical metallic nanowires*

Wu Ping(吴 平)[a], Xu Wen(徐 文)[a)b)†], Li Long-Long(李龙龙)[a], Lu Tie-Cheng(卢铁城)[c], and Wu Wei-Dong(吴卫东)[d]

[a] *Key Laboratory of Materials Physics, Institute of Solid State Physics, Chinese Academy of Sciences, Hefei* 230031, *China*
[b] *Department of Physics, Yunnan University, Kunming* 650091, *China*
[c] *Department of Physics, Sichuan University, Chengdu* 610064, *China*
[d] *Institute of Applied Electronics, China Academy of Engineering Physics, Mianyang* 621900, *China*

(Received 16 February 2014; revised manuscript received 22 April 2014; published online 20 August 2014)

We present a theoretical study on collective excitation modes associated with plasmon and surface-plasmon oscillations in cylindrical metallic nanowires. Based on a two-subband model, the dynamical dielectric function matrix is derived under the random-phase approximation. An optic-like branch and an acoustic-like branch, which are free of Landau damping, are observed for both plasmon and surface-plasmon modes. Interestingly, for surface-plasmon modes, we find that two branches of the dispersion relation curves converge at a wavevector $q_z = q_{\max}$ beyond which no surface-plasmon mode exists. Moreover, we examine the dependence of these excitation modes on sample parameters such as the radius of the nanowires. It is found that in metallic nanowires realized by state-of-the-art nanotechnology the intra- and inter-subband plasmon and surface-plasmon frequencies are in the terahertz bandwidth. The frequency of the optic-like modes decreases with increasing radius of the nanowires, whereas that of the acoustic-like modes is not sensitive to the variation of the radius. This study is pertinent to the application of metallic nanowires as frequency-tunable terahertz plasmonic devices.

Keywords: metallic nanowires, collective excitations, terahertz

PACS: 78.67.Uh, 73.20.Mf **DOI:** 10.1088/1674-1056/23/10/107807

1. Introduction

In recent years, plasmonics based on metallic nanowires (NWs) has received a great attention due to its potential applications in advanced electronic, magnetic, and optoelectronic devices.[1–3] In contrast to semiconductor-based NWs, in which plasmon oscillation plays an important role in influencing the electronic, optical, and optoelectronic properties mainly in the relatively low frequency regime, surface-plasmon excitation affects greatly the optical and optoelectronic properties of metallic NWs from the long- to short-wavelength regime. It is known that a surface plasmon is a kind of collective oscillation of a free electron gas at the interface between a metal and a dielectric material. Due to this unique feature, surface-plasmon modes can couple strongly with electromagnetic waves. Thus, a surface-plasmon polariton (SPP) can be achieved and the effect of surface-plasmon resonance (SPR) can be observed in metal-based device systems. In particular, the light waves can propagate along the metal–dielectric interface and can be modulated and guided by metallic nanostructures beyond the diffraction limit. Effects such as surface-enhanced Raman scatting (SERS) can be observed markedly in metallic nanostructures. Therefore, it is expected that the SPP and SPR in metallic nanostructures enable the nanoscale manipulation of the electromagnetic waves. This offers us a realistic solution in merging photonics and electronics at nanoscale dimensions.[4] The metallic nanostructures have been proposed as the fundamental building blocks for subwavelength plasmonics with potential applications in nanoscale optical components and devices.[5,6]

The metallic NWs and NW arrays are important categories of metallic nanostructures. In the past, plasmons in semiconductor-based NWs have been extensively studied both experimentally[7,8] and theoretically.[9,10] With the state-of-the-art nanotechnology, metallic NWs and NW arrays can be fabricated quite easily through, e.g., the electrochemical deposition of metals into porous anodic aluminum oxide templates,[11–13] and the pore diameter (or the diameter of the metal NWs) can be adjustable.[14] At present, less theoretical investigation has been carried out regarding surface plasmons in metallic NWs. Although surface-plasmonic effects in metal-based NW systems have been widely investigated experimentally, these elementary electronic excitations were mainly studied theoretically on the basis of classical theory, which cannot take fully into consideration the quantum size effects induced by the formation of the nanoscaled wire systems. In

*Project supported by the Funds from the Ministry of Science and Technology of China (Grant No. 2011YQ130018), the Funds from the Department of Science and Technology of Yunnan Province, the Open Research Fund Program of the State Key Laboratory of Low-Dimensional Quantum Physics (Grant No. KF201303), the Joint Research Fund from Sichuan University and China Academy of Engineering Physics, and the Funds from the Chinese Academy of Sciences (Grant No. YZ201223).

†Corresponding author. E-mail: wenxu_issp@aliyun.com

© 2014 Chinese Physical Society and IOP Publishing Ltd

the present study, we intend undertaking a detailed theoretical study employing the quantum theory to examine the plasmon and surface-plasmon modes in cylindrical metallic NWs. We would like to look into the different features of these plasmon and surface-plasmon modes in metallic NWs. Moreover, we would like to demonstrate theoretically how the basic features of plasmon and surface-plasmon modes in metallic NWs can be tuned by the radius of NWs realized by current nanotechnology.

2. Theoretical approaches

In this study, for simplicity we consider a cylindrical nanowire with infinite length in vacuum. Such a system can be realized by, e.g., firstly electrochemical depositing metal (e.g., Cu or Ni) into porous anodic alumina oxide templates,[11–13] then removing the template material via, e.g., chemical etching. We take the case where the conducting electrons are confined within a hard-well potential with cylindrical shape in the x–y plane and are free to move along the z axis of the wire. In cylindrical coordinates, the Schrödinger equation for an electron in this potential can be written as

$$\left[-\frac{\hbar^2}{2\mu}\left[\frac{1}{r}\frac{\partial}{\partial r}\left(r\frac{\partial}{\partial r}\right)+\frac{1}{r^2}\frac{\partial^2}{\partial\varphi^2}+\frac{\partial^2}{\partial z^2}\right]+V(r)\right]\psi(\boldsymbol{R}) = E\psi(\boldsymbol{R}). \tag{1}$$

Here $\boldsymbol{R}=(x,y,z)=(\boldsymbol{r},z)=(r,\varphi,z)$ and μ is the effective mass for an electron in the structure. In our model, the effective confining potential is modeled as

$$V(r)=\begin{cases}0, & r\le R_0,\\ \infty, & r>R_0,\end{cases} \tag{2}$$

where R_0 is the radius of the nanowire. This Schrödinger equation can be solved analytically. The electron wave function is obtained as

$$\psi_N(\boldsymbol{R})=\begin{cases}c_{nl}\mathrm{J}_{|l|}(q_{n|l|}r)\,\mathrm{e}^{(\mathrm{i}l\varphi+\mathrm{i}k_z z)}, & r\le R_0,\\ 0, & r>R_0,\end{cases} \tag{3}$$

with $N=(n,l,k_z)$ standing for all quantum numbers, $n=1,2,3,\ldots$, $l=0,\pm1,\pm2,\ldots$, and k_z being the wavevector for an electron moving along the z direction. Furthermore, $c_{nl}=[\sqrt{2}\pi R_0|\mathrm{J}_{|l|+1}(\beta_{n|l|})|]^{-1}$, $q_{nl}=\beta_{nl}/R_0$, and β_{nl} is the nth zero point for the Bessel function $\mathrm{J}_l(x)$. The corresponding eigenvalue is

$$E_N=\varepsilon_{nl}+\hbar^2k_z^2/2\mu, \tag{4}$$

with $\varepsilon_{nl}=\hbar^2q_{n|l|}^2/2\mu$. Such energy levels are twofold degenerate, namely $\varepsilon_{nl}=\varepsilon_{n|l|}$ if $l\neq0$. It is found that the lowest electronic subband has $n=1$ and $l=0$ and the first excited subband or second subband has $n=1$ and $l=\pm1$.

The matrix element for the bare electron–electron (e–e) interaction can be obtained by applying the single-electron wave function to the e–e interaction induced by the Coulomb potential, which reads

$$V_{N_1'N_1N'N} = \frac{e^2}{4\pi\kappa\varepsilon_0}\iint \mathrm{d}\boldsymbol{R}_1\,\mathrm{d}\boldsymbol{R}\;\psi_{N_1'}^*(\boldsymbol{R}_1)\psi_{N_1}(\boldsymbol{R}_1) \times\frac{1}{|\boldsymbol{R}_1-\boldsymbol{R}|}\psi_{N'}^*(\boldsymbol{R})\psi_N(\boldsymbol{R}). \tag{5}$$

Here κ is the high-frequency dielectric constant of the metallic nanowire and ε_0 is the vacuum permittivity. Setting $j=(n,l)$, we have

$$V_{N_1'N_1N'N}=\upsilon_{j_1'j_1j'j}(q_z)\delta_{k_z',k_z+q_z}\delta_{k_{z_1}',k_{z_1}-q_z}\delta_{l_1+l,l_1'+l'}, \tag{6}$$

where q_z is the change of electron wavevector or momentum during an e–e interacting event,

$$\upsilon_{j_1'j_1j'j}(q_z)=\frac{e^2}{4\pi\kappa\varepsilon_0}c_{j_1'j_1j'j}\mathbb{R}_{j_1'j_1j'j}(q_z), \tag{7}$$

with $c_{j_1'j_1j'j}$ and $\mathbb{R}_{j_1'j_1j'j}(q_z)$ being

$$c_{j_1'j_1j'j} = 4\big|\pi\mathrm{J}_{|l_1'|+1}(\beta_{n_1'|l_1'|})\mathrm{J}_{|l_1|+1}(\beta_{n_1|l_1|}) \times\mathrm{J}_{|l'|+1}(\beta_{n'|l'|})\mathrm{J}_{|l|+1}(\beta_{n|l|})\big|^{-1} \tag{8}$$

and

$$\mathbb{R}_{j_1'j_1j'j}(q_z) = R_0^{-4}\int_0^{R_0}\int_0^{R_0}\mathrm{d}r_1\,\mathrm{d}r\,r_1r\mathrm{J}_{|l_1'|}(q_{n_1'|l_1'|}r_1)\mathrm{J}_{|l'|}(q_{n'|l'|}r) \times\mathrm{J}_{|l_1|}(q_{n_1|l_1|}r_1)\mathrm{J}_{|l|}(q_{n|l|}r)\mathrm{I}_m(q_zr_<)\mathrm{K}_m(q_zr_>). \tag{9}$$

Here, $m=||l'|-|l||$, $\mathrm{I}_m(x)$ and $\mathrm{K}_m(x)$ are the mth modified Bessel functions of the first and the second kind, and $r_<$ ($r_>$) is the smaller (larger) of $\{r,r_1\}$.

With electronic energy spectrum obtained by solving the Schrödinger equation, we can derive the retarded and advanced Green functions for electrons. Applying these Green functions to the diagrammatic techniques, the effective e–e interaction can be derived under the random phase approximation (RPA). The matrix element of dynamical dielectric function is then obtained as[15]

$$\varepsilon_{\alpha\beta}(\Omega,q_z)=\delta_{\alpha,\beta}-V_{\alpha\beta}\Pi_\beta(\Omega,q_z), \tag{10}$$

where $\alpha=N'N$ and the density–density (d–d) correlation function in the absence of e–e interaction is

$$\Pi_{N'N}(\Omega,q_z)=g_\mathrm{s}\sum_{k_z}\frac{f(E_{N'})-f(E_N)}{\hbar\Omega+E_{N'}-E_N+\mathrm{i}\delta}, \tag{11}$$

with $g_\mathrm{s}=2$ being the spin degeneracy and $f(E)$ the Fermi–Dirac function.

To solve the complicated algebraic equation, Eq. (10), which determines the dispersion relation of the collective excitations, it is necessary to restrict the discussion to a finite number of subbands. Here, we use the two-subband model,

which has been successfully applied to deal with semiconductor quantum-wire systems in the case where only the lowest electronic subband is occupied.[10] With this simple and tractable theoretical model, we can reveal the fundamental characteristics of the intra- and inter-subband collective excitations. In the present study, we consider that only the lowest electronic subband ε_{10} is occupied by electrons. After setting $j = + = (1,0)$ and $- = (1,\pm 1)$, $p = (j'j) = 1 = (++)$, $2 = (+-)$, $3 = (-+)$, and $4 = (--)$, the dielectric function matrix for a two-subband model is

$$\varepsilon(\Omega, q_z) = \begin{pmatrix} 1+a_{11} & 0 & 0 & a_{14} \\ 0 & 1+a_{22} & a_{23} & 0 \\ 0 & a_{32} & 1+a_{33} & 0 \\ a_{41} & 0 & 0 & 1+a_{44} \end{pmatrix}, \quad (12)$$

with $a_{p_1 p} = -\upsilon_{p_1 p}(q_z)\Pi_p(\Omega, q_z)$ $(p = j'j)$ and

$$\Pi_p(\Omega, q_z) = g_j g_{j'} g_s \sum_{k_z} \frac{f(E_{j'k_z+q_z}) - f(E_{jk_z})}{\hbar\Omega + E_{j'k_z+q_z} - E_{jk_z} + i\delta}, \quad (13)$$

where $g_j = 1$ or 2 is the angular quantum number degeneracy for $j = +$ or $-$, $\Pi_4 = \Pi_{--}(\Omega, q_z) = 0$ because the second subband is unoccupied, and therefore $a_{14} = a_{44} = 0$. Some matrix elements vanish because of the selection rule $\delta_{l+l_1,l'+l'_1}$ in Eq. (6). Since $\upsilon_{23}(q_z) = \upsilon_{32}(q_z)$, the determinant of the dielectric function matrix is given as

$$\begin{aligned} \|\varepsilon(\Omega, q_z)\| = {} & \{1 - \upsilon_{11}(q_z)\Pi_1(\Omega, q_z)\}\{1 - \upsilon_{23}(q_z) \\ & \times [\Pi_2(\Omega, q_z) + \Pi_3(\Omega, q_z)]\}, \end{aligned} \quad (14)$$

which is induced by intra- and inter-subband transition events. In the low-temperature limit (i.e., $T \to 0$), we obtain

$$\mathrm{Re}\Pi_1(\Omega, q_z) = \frac{A}{q_z} \ln \left| \frac{(K_+)^2 - (\mu\Omega/\hbar q_z)^2}{(K_-)^2 - (\mu\Omega/\hbar q_z)^2} \right|, \quad (15)$$

$$\mathrm{Re}\Pi_2(\Omega, q_z) = \frac{2A}{q_z} \ln \left| \frac{K_+ + \Delta - \mu\Omega/\hbar q_z}{K_- + \Delta - \mu\Omega/\hbar q_z} \right|, \quad (16)$$

and

$$\mathrm{Re}\Pi_3(\Omega, q_z) = \frac{2A}{q_z} \ln \left| \frac{K_+ + \Delta + \mu\Omega/\hbar q_z}{K_- + \Delta + \mu\Omega/\hbar q_z} \right|, \quad (17)$$

with $A = -\mu/\pi\hbar^2$, $K_\pm = \pm k_\mathrm{F} + q_z/2$, $k_\mathrm{F} = \pi n_\mathrm{e}/2$ is the Fermi wavevector, n_e is the electron density, and $\Delta = (\beta_{11}^2 - \beta_{10}^2)/(2q_z R_0^2)$. The plasmon and surface-plasmon modes are determined, respectively, by Ref. [16]: $\mathrm{Re}\|\varepsilon(\Omega, q_z)\| \to 0$ and $\mathrm{Re}\|\varepsilon(\Omega, q_z)\| \to -1$.

3. Results and discussion

For numerical calculations in the present study, we take the typical electron density as $n_\mathrm{e} = 10^6$ cm^{-1} and the low-temperature limit $T \to 0$ K. At this electron density, we find that the second electronic subband becomes occupied when $R_0 > 20$ nm. In conjunction with the metallic NWs realized from the electrochemical deposition of metals into porous anodic alumina oxide templates,[11–13] we consider Cu-based NW systems. We take the effective mass for an electron as $\mu \simeq 1.49 m_\mathrm{e}$, and the high-frequency dielectric constant as $\kappa = 6.0$ for Cu-based NWs.[17]

For $\mathrm{Re}\|\varepsilon(\Omega, q_z)\| = 0$ in Eq. (14), we get two equations: $1 - \upsilon_{11}(q_z)\mathrm{Re}\Pi_1(\Omega, q_z) = 0$, or $1 - \upsilon_{23}(q_z)[\mathrm{Re}\Pi_2(\Omega, q_z) + \mathrm{Re}\Pi_3(\Omega, q_z)] = 0$, which determine the plasmon modes induced by intra- and inter-subband electronic transition events, respectively. The surface-plasmon modes are determined by $\mathrm{Re} \parallel \varepsilon(\Omega, q_z) \parallel = -1$ and, as a result, the intra- and inter-subband excitation modes are coupled to each other.

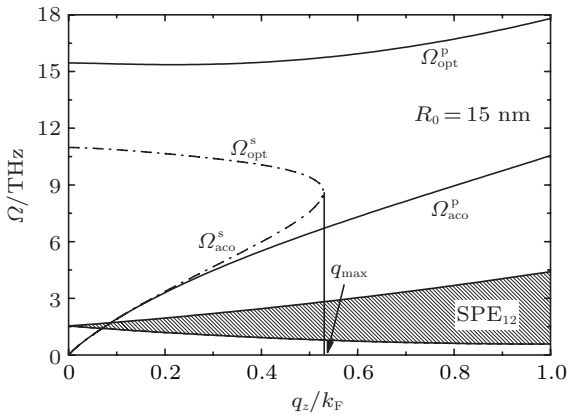


Fig. 1. The dispersion relation of plasmon and surface-plasmon modes in a metallic nanowire with a radius $R_0 = 15$ nm. Here, $\Omega^\mathrm{p}_\mathrm{opt}$ ($\Omega^\mathrm{s}_\mathrm{opt}$) and $\Omega^\mathrm{p}_\mathrm{aco}$ ($\Omega^\mathrm{s}_\mathrm{aco}$) represent the optic-like and acoustic-like branches of the plasmon (surface-plasmon) modes, respectively. The shaded area (SPE$_{12}$) shows the spectrum for single-particle excitation induced by inter-subband transition between the first and second subbands. q_max is the maximum wavevector beyond which the surface-plasmon mode is not present.

In Fig. 1, we show the dispersion relation of the plasmon and surface-plasmon modes for a metallic NW with a radius $R_0 = 15$ nm. We find that using the two-subband model under which only the lowest electronic subband is occupied and the second subband is empty, two branches of plasmon and surface-plasmon modes can be observed. One branch is acoustic-like where $\Omega^\mathrm{p}_\mathrm{aco} \to 0$ and $\Omega^\mathrm{s}_\mathrm{aco} \to 0$ as $q_z \to 0$ and the plasmon and surface-plasmon frequencies depend strongly on wavevector q_z. Another branch is optic-like, where $\Omega^\mathrm{p}_\mathrm{opt}$ and $\Omega^\mathrm{s}_\mathrm{opt}$ are finite as $q_z \to 0$ and the plasmon and surface-plasmon frequencies depend relatively weakly on wavevector q_z in the small q_z regime. In the small $q_z/k_\mathrm{F} \ll 1$ regime, the dispersion relations for acoustic-like plasmon and surface-plasmon modes are roughly the same. With increasing q_z, the acoustic-like branch of the surface-plasmon modes ($\Omega^\mathrm{s}_\mathrm{aco}$) lies above that of the plasmon modes ($\Omega^\mathrm{p}_\mathrm{aco}$) and their frequency separation ($\Omega^\mathrm{s}_\mathrm{aco} - \Omega^\mathrm{p}_\mathrm{aco}$) increases. The frequency of the optic-like surface-plasmon mode ($\Omega^\mathrm{s}_\mathrm{opt}$) is obviously lower than that of the optic-like plasmon mode ($\Omega^\mathrm{p}_\mathrm{opt}$). With increasing q_z,

Ω^{p}_{opt} increases whereas Ω^{s}_{opt} decreases. As can be seen from Fig. 1, the two branches of the surface-plasmon modes converge at one point $q_z = q_{max}$ and the surface-plasmon mode vanishes when $q_z > q_{max}$. That is, the surface-plasmon modes only exist within $q_z < q_{max}$ in nanowire systems. Such an interesting effect is caused mainly by the coupling between intra- and inter-subband electronic transition channels for excitation of surface-plasmon modes. In Fig. 1, the shaded area (SPE_{12}) shows the spectrum of single-particle excitation (SPE) induced by inter-subband electronic transition channels. In the SPE_{12} region, the imaginary part of the dielectric function matrix element induced by electronic transition between the first and second subbands is nonzero. This implies that Landau damping and optical absorption can occur in this region. Because the frequency of SPE for intra-subband transition is much smaller than that for inter-subband transition, we do not show the spectrum of SPE for intra-subband transition in Fig. 1 for simplicity. It is clear that all plasmon and surface-plasmon modes shown in Fig. 1 are out of the area of the SPE. Consequently, the plasmon and surface-plasmon modes induced by intra- and inter-subband electronic transition channels in metallic NWs are free of Landau damping. Moreover, as can be seen from Fig. 1, for metallic NWs with the radius $R_0 \sim 15$ nm, the frequencies of plasmon and surface-plasmon modes induced by intra- and inter-subband transition channels are in the terahertz (10^{12} Hz or THz) optical bandwidth. This indicates that the metallic NWs and NW arrays may be applied as THz plasmonic devices.

In Fig. 2, we show the dispersion relation of the plasmon (a) and the surface-plasmon (b) modes for different radii of the metallic NWs as indicated. We notice that the frequencies of optic-like branches for both plasmon and surface-plasmon modes decrease monotonically with increasing NW radius R_0. This is because the energy separation between the first and second subbands is inversely proportional to R_0^2 (see Eq. (4)). Due to the fact that the frequencies of optic-like plasmon and surface-plasmon modes are determined by the energy spacing between two subbands, the corresponding excitation frequencies become smaller as the NW radius increases. In contrast, the frequencies of acoustic-like branches for plasmon and surface-plasmon modes depend relatively weakly on the variation of the NW radius since the acoustic-like modes are induced by the intra-subband electronic transition events. With decreasing radius R_0, q_{max} becomes larger. This indicates that the surface-plasmon modes can exist in a wider wavevector range in metallic NWs. These results shown in Fig. 2 demonstrate theoretically that we can tune effectively the frequencies of plasmon and surface-plasmon modes within the THz bandwidth by simply altering the diameter of the metallic NWs.

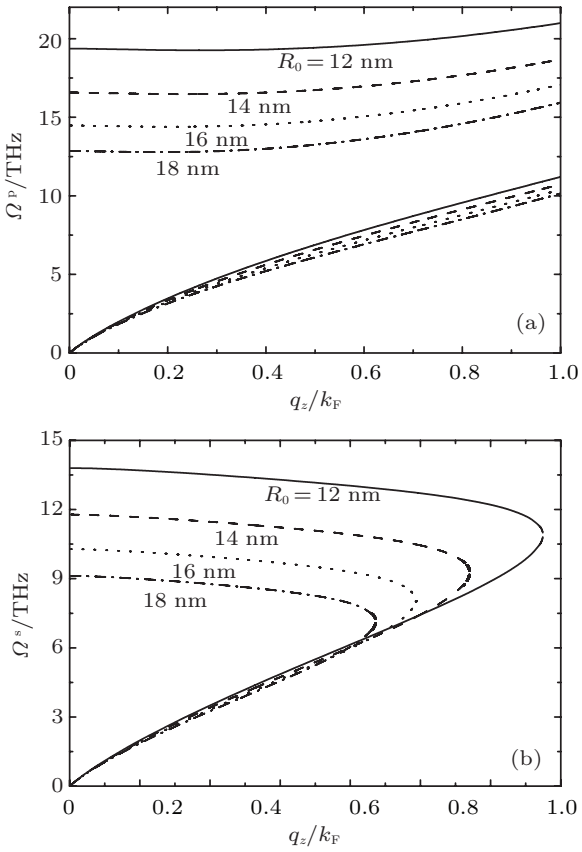


Fig. 2. The dispersion relation of (a) plasmon and (b) surface-plasmon modes for different NW radii R_0 as indicated.

In the present study, we take a two-subband model to examine the plasmon and surface-plasmon modes in metallic NWs. The inclusion of more electronic subbands within the calculation can only result in the observation of optic-like collective excitation modes in the higher frequency regime. The results obtained from this study indicate that, in metallic NWs realized from state-of-the-art nanotechnology, THz plasmon and surface-plasmon modes can be present without Landau damping. It is well known that THz technology is of great potential for many applications in extensive fields such as biological science, sensing, imaging, and spectroscopy.[18] The application of metallic nanostructured materials in THz technology has become an important and fast-growing field of research in recent years. It has been demonstrated experimentally that the generation of THz signal from metallic nanoparticle array systems can be achieved due to surface-plasmon excitation.[19] We propose that the metallic NW systems could also be used as THz sources or detectors with the advantage that they can be easily fabricated with the state-of-the-art nanotechnology. The plasmons and surface plasmons present in the NWs can strongly couple with the electromagnetic modes under appropriate conditions to form so-called plasmon polariton and surface-plasmon polaritons. Therefore, one may anticipate THz emission originating from the radiative decay of the plasmon and surface-plasmon polaritons in metallic

NW structures because the intra- and inter-subband plasmon and surface-plasmon modes are within the THz bandwidth. Moreover, the detection of the THz radiation through the resonant absorption of THz radiation by excitation of plasmon and surface-plasmon polaritons can be achieved. As is well known, the work frequencies of THz optoelectronic devices are usually within a few THz. However, for metallic NW systems, our theoretical results indicate that the frequency region of the plasmon and surface-plasmon modes can be extended to dozens of THz. Hence, it is possible to realize broadband and high-frequency THz emitters and detectors based on metallic NW and NW array systems.

4. Conclusions

In this study, we have theoretically studied the collective excitations associated with plasmon and surface-plasmon modes in cylindrical metallic NW systems. Using a two-subband model, the dynamical dielectric function matrix has been derived within the RPA approach and, from it, we have examined the dispersion relation of plasmon and surface-plasmon modes induced by intra- and inter-subband electronic transition channels in NWs. We have found that two branches of each collective excitation mode can be observed, and all of them are free of Landau damping. For plasmon modes, the optic-like branch induced by inter-subband transition and the acoustic-like branch induced by intra-subband transition can be found. More interestingly, for surface-plasmon modes we have shown that two branches of the dispersion relation curves converge at one wavevector point $q_z = q_{\max}$. The surface-plasmon mode is not present for $q_z > q_{\max}$. Such an effect is caused mainly by the fact that the surface-plasmon excitation in metallic NWs is achieved by the coupling between the intra- and inter-subband electronic transition channels. The acoustic-like branches for both the plasmon and surface-plasmon modes look roughly the same in the small q_z regime; however, the frequencies of the optic-like surface-plasmon modes are obviously lower than those of the plasmon modes. We have examined the dependence of these collective excitation modes on the radius of metallic NWs. It has been found that the frequencies of optic-like plasmon and surface-plasmon modes can be tuned effectively by simply altering the radius of the NWs. The acoustic-like branches of these modes depend relatively weakly on the NW radius. The most important conclusion we drew from this study is that THz plasmon and surface-plasmon modes can be present in the metallic NW systems realized from state-of-the-art nanotechnology. This opens the opportunity to seek applications of metallic nanowires as frequency-tunable plasmonic devices.

References

[1] Lal S, Hafner J H, Halas N J, Link S and Nordlander P 2012 *ACC Chem. Res.* **45** 1887
[2] Fan X X, Hu H N, Zhou S M, Yang M, Du J and Shi Z 2012 *Chin. Phys. Lett.* **29** 077802
[3] Lee J Y, Connor S T, Cui Y and Peumans P 2008 *Nano Lett.* **8** 689
[4] Ozbay E 2006 *Science* **311** 189
[5] Li Z P, Zhang S P, Halas N J, Nordlander P and Xu H X 2011 *Small* **7** 593
[6] Zhu Y, Wei H, Yang P F and Xu H X 2012 *Chin. Phys. Lett.* **29** 077302
[7] Egeler T, Abstreiter G, Weimann G, Demel T, Heitmann D, Grambow P and Schlapp W 1990 *Phys. Rev. Lett.* **65** 1804
[8] Demel T, Heitmann D, Grambow P and Ploog K 1991 *Phys. Rev. Lett.* **66** 2657
[9] Huang F Y 1990 *Phys. Rev. B* **41** 12957
[10] Wendler L and Grigoryan V G 1994 *Phys. Rev. B* **49** 14531
[11] Xu S H, Fei G T, Zhu X G, Wang B, Wu B and Zhang L D 2011 *Nanotechnology* **22** 265602
[12] Zhou W F, Fei G T, Li X F, Xu S H, Chen L, Wu B and Zhang L D 2009 *J. Phys. Chem. C* **113** 9568
[13] Yang Y W, Li T Y, Zhu W B, Ma D M and Chen D 2013 *Chin. Phys. Lett.* **30** 108102
[14] Liu J, Duan J L, Toimil-Molares M E, Karim S, Cornelius T W, Dobrev D, Yao H J, Sun Y M, Hou M D, Mo D, Wang Z G and Neumann R 2006 *Nanotechnology* **17** 1922
[15] Xu W, Das M D and Lin L B 2003 *J. Phys.: Condens. Matter* **15** 3249
[16] Xiao Y M, Xu W, Zhang Y Y and Hu J G 2012 *Nanoscale Res. Lett.* **7** 578
[17] Johnson P B and Christy R W 1972 *Phys. Rev. B* **6** 4370
[18] Kawase K, Ogawa Y and Watanabe Y 2003 *Opt. Express* **11** 2549
[19] Polyushkin D K, Hendry E, Stone E K and Barnes W L 2011 *Nano. Lett.* **11** 4718